Journal of Materials Chemistry C, 2015,**3**, 1694-1699. **DOI:** 10.1039/C4TC02381A

A giant electrocaloric effect of a $Pb_{0.97}La_{0.02}(Zr_{0.75}Sn_{0.18}Ti_{0.07})O_3$ antiferroelectric thick film at room temperature

Ye Zhao[1], Xihong Hao[*,1], and Qi Zhang[2,3]

1-School of Materials and Metallurgy, Inner Mongolia University of Science and Technology, Baotou 014010, China

2-State Key Laboratory of Advanced Technology for Materials Synthesis and Processing, Wuhan University of Technology, Wuhan 430070, Hubei, China

3-Department of Manufacturing and Materials, Cranfield University, Cranfield, Bedfordshire, MK43 0AL, UK

Abstract: A 2-μm-$Pb_{0.97}La_{0.02}(Zr_{0.75}Sn_{0.18}Ti_{0.07})O_3$ (PLZST) antiferroelectric (AFE) thick film with tetragonal structure was deposited on $LaNiO_3$/Si (100) substrates via a sol-gel technique. The electrocaloric effect (ECE) of the PLZST thick film is investigated under the functions of external electric field and temperature. Giant ECEs (ΔT = 53.8 °C and ΔS = 63.9 $J \cdot K^{-1} \cdot kg^{-1}$) are received at 5 °C, which is attributed to a field-induced AFE to ferroelectric (FE) phase transition. Moreover, a large ΔT of above 30 °C is remains at temperature range from 5 °C to 25 °C. The maximum electrocaloric coefficient (ξ_{max} = 0.060 K·cm/kV) and refrigeration efficiency (COP = 18) of the film are also obtained at 5 °C. At room temperature, the values of ΔT, ΔS, COP and ξ_{max} are 35.0 °C, 39.0 $J \cdot K^{-1} \cdot kg^{-1}$, 14 and 0.039 K·cm/kV at 900 kV/cm, respectively. The AFE thick films with giant ECEs are promising candidates for applications in cooling systems at room temperature.

Keywords: ECE, PLZST AFE thick film, AFE-FE phase transition, room temperature

*Corresponding author: xhhao@imust.cn; Tel: +86-472-5951572; Fax: +86-472-5951571

1. Introduction

The electrocaloric effect (ECE) is a reversible change in the temperature of a material upon application or withdrawal of an electric field under adiabatic condition.[1-6] The large ECE may provide an efficient means to realize solid-state cooling devices for a broad range of applications such as on-chip cooling and temperature regulation for sensors and electronic devices.[7-8] The first study on ECE was reported in 1930 in Rochelle salt by Kobeko and Kurtschatov, however no numerical values were reported in these works.[9] In 1963, Wiseman and Kuebler redid their measurements, obtaining ECE of 0.0036 ^{o}C in an electric field of 1.4 kV/cm at 22.2 ^{o}C.[10] In the 1960s to 1970s, a great interest was generated in the bulk electrocaloric materials. Nevertheless, the observed ECE was very weak because of the low breakdown electric field of bulk materials, which could not meet the request of commercial application. For example, the highest ECE was only 2.5 K in $Pb_{0.99}Nb_{0.02}(Zr_{0.75}Sn_{0.20}Ti_{0.05})_{0.98}O_3$ bulk ceramic.[11] Thus, it was predicated that an improved ECEs could be realized in the thin films, because of their good electric-field endurance. As expected, giant ECE of 12 K at 25 V and 31 K at 18 V were reported in 350-nm-thick $PbZr_{0.95}Ti_{0.05}O_3$ film and in 240-nm-thick $0.65PbMg_{1/3}Nb_{2/3}O_3$-$0.35PbTiO_3$ film, respectively.[7,12] These results have inspired the research interest on ECE-based solid-state cooling devices. However, because of the small thickness (< 1 μm), the overall heat-sinking capacity of the thin films was still insufficient for practical applications and cannot be commercially exploited. As a result, it could be concluded that, due to the higher breakdown electric field and larger overall volume, thick films (1-100 μm) might overcome the shortcomings of bulk ceramics and thin films and are suitable for the applications in cooling devices. Meanwhile, large ECE at near room temperatures is also desirable for cooling device applications.

Assuming the reversible adiabatic changes following Maxwell relation $\left(\frac{\partial P}{\partial T}\right)_E = \left(\frac{\partial S}{\partial E}\right)_T$, the temperature change ΔT and entropy change ΔS for a material of density ρ with specific heat capacity C are expressed as follows:[13]

$$\Delta T = -\frac{1}{C\rho}\int_{E_1}^{E_2} T\left(\frac{\partial P}{\partial T}\right)_E dE , \quad (1)$$

$$\Delta S = -\frac{1}{\rho}\int_{E_1}^{E_2}\left(\frac{\partial P}{\partial T}\right)_E \mathrm{d}E , \quad (2)$$

where T is operating temperature, P is maximum polarization at applied electric field E, and E_1 and E_2 are the initial and final applied electric field, respectively. Evidently, the materials, which possess a larger $\left(\frac{\partial P}{\partial T}\right)_E$, would also have higher ECEs. Currently, the studies on ECE were mainly focused on the phase-transition process from FE (or AFE) phase to paraelectric (PE) phase. Taking FEs as an example, the application of an external electric field to a FE will promote the degree of order of the dipoles, which leads to the decrease of entropy and the increase of temperature. Reversely, in an isothermal condition, the temperature of FEs is reduced upon the withdrawal of the external electric field, companied by an increase of entropy, as shown in Fig. 1(a). Because of the large entropy change, the maximum ECE is often observed near the Curie temperature, corresponding to the FE/AFE-PE phase transition.[14]

In fact, the phase transition between AFE and FE could also bring a large entropy change. As a result, a large temperature change could also be obtained during FE-AFE transition upon the withdrawal of electric field, as shown in Fig. 1(b). Moreover, it was reported that the magnitude of $\left(\frac{\partial P}{\partial T}\right)_E$ was much higher from FE-AFE transition than that from FE/AFE to PE transition.[15] Meanwhile, the phase transition of FE-AFE induced sufficiently external electric filed is easily

realized at near room temperatures, while the phase transition of AFE/FE-PE usually occurs at the high temperature. Therefore, it is predicated that larger ECE in AFEs could possibly be realized at near the room temperatures. The first work on the ECE in AFEs was reported by Thacher in 1968, in which a temperature change of ΔT = 1.6 K at 328 K in $Pb(Zr_{0.455}Sn_{0.455}Ti_{0.09})O_3$ bulk ceramics was observed during FE-AFE phase switching.[16] Recently, a giant ECE peak (ΔT =45.3 K) at room temperature was reported in a 320-nm-thick $Pb_{0.8}Ba_{0.2}ZrO_3$ (PBZ) thin film.[13] However, the temperature range of ECE peak of $Pb_{0.8}Ba_{0.2}ZrO_3$ film was slightly narrow, possibly due to the weak AFE nature of PBZ film. These results indicate that it is possible to obtain large ECE at a wide operating range at the phase transition between AFE and FE near room temperature by properly controlling the composition of AFEs. $Pb(Zr,Sn,Ti)O_3$ family in AFE materials have been studied extensively over past several decades. A small amount of La doping into the $Pb(Zr,Sn,Ti)O_3$ material was found to lead the dispersion behavior in both the ferroelectric rhombohedral and tetragonal states, and to increase the stability range of the AFE state.[17]

Thus, in this work, a tetragonal $Pb_{0.97}La_{0.02}(Zr_{0.75}Sn_{0.18}Ti_{0.07})O_3$ thick film with pure AFE phase was prepared, and the electric field-dependent ECE resulted from the phase transition between AFE and FE was investigated. The aim of this study is to investigate the ECE of the PLZST thick film at phase transition from AFE to FE at room temperature and their heat-sinking capacity.

2. Results and Discussion

Fig. 2 shows a XRD pattern of the tetragonal PLZST AFE thick film after annealing at 700 ^{o}C. The result indicates that the PLZST AFE thick film is well crystallized into a pure polycrystalline perovskite phase. For convenience, the lattice indexes of the peaks are labeled as pseudocubic structure (the parent perovskite structure) rather than the tetragonal structure. The results followed

Xu's reports of PLZST thick film [17]. The FE-SEM morphology of the thick film surface is shown in the inset in Fig. 2(a). It is observed that the film possesses a compact and uniform morphology. The so-called "rosette" structure of surface morphology is not observed, which is consistent with the result in Pb-containing films derived from PVP-modified sol-gel solutions.[18] The inset in Fig. 2(b) presents the cross-section image of the film. The thickness of the film determined from the cross-section picture is about 2 μm. The film has a granular microstructure with significant amounts of nanosized pores, probably due to the decomposition of PVP in the heat treatment process. The similar results were reported in the PLZT thick films by Park.[19]

Temperature dependences of the dielectric constant for the PLZST AFE thick film are shown in Fig. 3, which were measured at 1, 10, and 100 kHz on heating process. The Curie temperature (T_c) of the film is 195 °C, which is close to that (T_c = 170 °C) of $Pb_{0.97}La_{0.02}(Zr_{0.75}Sn_{0.15}Ti_{0.10})O_3$ AFE bulk ceramics with the similar composition.[20] The inset in Fig. 3 presents the room temperature frequency-dependent dielectric constant and dielectric loss of the thick film, which were measured at 1-1000 kHz. Obviously, as the frequency increase, the dielectric constant of the film is slightly fluctuated. Moreover, the thick film exhibits small loss tangent of below 0.057, which is attributed the uniform microstructure.

The Fig. 4 plots the *P-E* loops of the film at 25 °C, 95 °C and 195 °C, which were measured at 1 kHz and at 600 kV/cm. The film displays a slanted and double *P-E* loop with a large maximum polarization and a small remnant polarization at room temperature, which represented the gradual change in polarization and a diffused phase switching between the AFE and the FE phases. With the measuring temperature increasing, the tetragonal PLZST AFE thick film changes into PE phase, confirmed by the *P-E* loops. The dielectric constant of the PLZST thick film was measured as a

function of a slowly varying dc bias applied field at 100 kHz. As shown in the inset of Fig. 4 the double butterfly behavior in dielectric constant vs. an applied electric field demonstrates the AFE nature and the field-induced transition into the FE characteristics of the film. The forward phase switching (AFE-to-FE) field (E_F) is approximately 130 kV/cm and the backward phase switching (FE-to-AFE) field (E_A) is approximately 80 kV/cm for the thick film.

Fig. 5(a) shows the adiabatic temperature changes ΔT of the PLZST thick film under different electric field, which was calculated by using Equation 1. In this work, values of $\left(\frac{\partial P}{\partial T}\right)_E$ were obtained from fourth-order polynomial fits to raw *P (T)* data extracted from the upper branches of *P-E* loops in $E > 0$, as shown in inset of Fig. 5(a). The specific heat capacity C = 330 $J \cdot K^{-1} \cdot kg^{-1}$ remains constant for Zr-rich lead-based films and the peak associated with the transition is < 10% of the background.[21] The theoretical density ρ = 8.3 $g \cdot cm^{-3}$ was selected for the film, which was similar to the previous report.[7] As expected, the maximum ΔT = 53.8 °C at 5 °C was received at the applied electric field E = 900 kV/cm, which was induced by the phase transition of FE-AFE. A large ΔT of above 30 °C was remained at temperature range from 5 °C to 25 °C. With the operating temperature increasing, the ΔT firstly decreases, indicating a reduction of entropy change between AFE and FE phase transition. With the further increase of temperature, the peak of ΔT = 13 °C was observed at 175 °C at E = 900 kV/cm, which was supposed to be caused by the AFE-PE phase transition. The temperature corresponding to the peak of ΔT was the slightly below its T_c, which was consistent with previous report by Tatsuzaki, because the spontaneous value of P changes with temperature below T_c.[22] In fact, ECE can occur both above and below T_c, but microscopic models of ECEs are not well established.[7] Fig. 5(b) shows the corresponding adiabatic entropy changes (ΔS) of the PLZST AFE thick film under different electric field. Clearly, the maximum ΔS value of 63.9

$J \cdot K^{-1} \cdot kg^{-1}$ was obtained at 5 °C at 900 kV/cm, which higher than that (32 $J \cdot K^{-1} \cdot kg^{-1}$) in $Pb(Mg_{1/3}Nb_{2/3})_{0.65}Ti_{0.35}O_3$ thin film and that (60 $J \cdot K^{-1} \cdot kg^{-1}$) in FE polymer [P(VDF-TrFE)] (55/45 mol%) films.[12,23] At room temperature (25 °C), the value of ΔS is 39.0 $J \cdot K^{-1} \cdot kg^{-1}$. The large ΔS of the PLZST thick film induces a large ECE, which is required in cooling system.

In order to give a comparison criterion for electrocaloric refrigeration, the Fig. 6 shows the materials efficiency (*COP*) and electrocaloric coefficient (ξ_{max}) of the PLZST AFE thick film at 900 kV/cm and at different temperatures. Following Defay's study, [24] the refrigeration efficiency is defined as:

$$COP = \frac{|Q|}{|W|} = \frac{|\Delta S \times T|}{|W|} \quad (3),$$

$$W = \int_{P_r}^{P_{max}} EdP \quad (4),$$

where Q is isothermal heat and *W* is energy-storage density. Based on above formulas, the maximum *COP* of the AFE thick film is found to be 18 at 5 °C at 900 kV/cm. Electrocaloric coefficient is defined as $\xi_{max} = \Delta T_{max}/\Delta E_{max}$, where ΔT_{max} is the maximum temperature change, and ΔE_{max} is the corresponding electric field change. Clearly, the maximum ξ_{max} of the film is 0.060 K·cm/kV at 5 °C. The change of *COP* and ξ_{max} is in agreement with ΔT of the thick film, as a function temperature. At room temperature, the values of *COP* and ξ_{max} are 14 and 0.039 K·cm/kV at 900 kV/cm, respectively. For comparison, Table 1 lists the ECE characteristics of the films, polymer, ceramics and single crystals, including PLZST, $PbZr_{0.95}Ti_{0.05}O_3$,[7] P(VDF-TrFE), P(VDF-TrFE-CFE),[23] $Pb_{0.80}Ba_{0.20}ZrO_3$,[13] 0.85PMN-0.15PT films,[25] and $Pb_{0.99}Nb_{0.02}(Zr_{0.75}Sn_{0.20}Ti_{0.05})_{0.98}O_3$,[11] $Pb(Zr_{0.455}Sn_{0.455}Ti_{0.09})O_3$,[16] $BaZr_{0.2}Ti_{0.8}O_3$,[4] PZT-5,[26] $0.94Na_{0.5}Bi_{0.5}TiO_3$–$0.06KNbO_3$,[27] $Pb(Mg_{0.067}Nb_{0.133}Zr_{0.8})O_3$ ceramics,[28] and $0.45Ba_{0.2}Ti_{0.8}O_3$-$0.55Ba_{0.7}Ca_{0.3}TiO_3$ single crystal.[29]

Refrigerant capacity (*RC*) is also an important parameter, which is a measurement of how much heat can be transferred between the cold and hot sinks in an ideal refrigerant cycle. The *RC* is defined as RC = $\Delta S \times \Delta T$.[30] As can be seen, the ΔT, *COP*, and *RC* of the PLZST thick film are the largest among all the films, except ξ_{max}. The combination of these high values indicates the potential of the PLZST AFE thick film for the ECE based cooling devices with high cooling efficiency.

Fig. 7 shows the leakage current density and the resistivity as a function of time for E = 900 kV/cm at 5 °C, 25 °C, 95 °C and 175 °C， respectively. Clearly, the leakage current density shows strong initial-time dependence because of the dielectric polarization relaxation, which obeys the Curie-von Schweidler law as follows [31]:

$$J = J_s + J_0 \times t^{-n}, \quad (8)$$

where J_s is the steady-state current density, J_0 is a fitting constant, t is the relaxation time in second, and n is the slope of the log-log plot. There possible mechanisms are associated with the Curie-von Schweidler law: space charge trapping, relaxation time distribution and electrical charge hopping [32]. Obviously, the leakage current density of the film increases with increasing temperature. Moreover, the resistivity of the thick film displays a rising trend in the measurement range. For example, the resistivity is 7.1×10^{13}, 1.3×10^{13}, 0.5×10^{13}, and 0.4×10^{13} Ωm at 5 °C, 25 °C, 95 °C and 175 °C, respectively. The inset of Fig. 7 shows the corresponding temperature dependences of steady-state leakage current density, which are 0.9, 5.1, 12.4, and 14.6 μA/cm^2 for the film at 5 °C, 25 °C, 95 °C and 175 °C, respectively. The small leakage current yields negligible Joule heating of ~ 10^{-3} K and does not affect *P-E* results because currents of hundreds of μA are required to switch the measured polarizations at 1 kHz.

3. Experimental

The composition of $Pb_{0.97}La_{0.02}(Zr_{0.75}Sn_{0.18}Ti_{0.07})O_3$ (PLZST) was selected to study, which locates in tetragonal region. The PLZST precursor solution was synthesized using lead acetate trihydrate, lanthanum acetate, tin acetate, titanium isopropoxide and zirconium isopropoxide as the starting raw materials. Glacial acetic and deionized water were used as solvents. 20 mol% excess of lead acetate trihydrate was introduced to compensate the lead loss during annealing and to prevent the formation of pyrochlore phase in the film. In order to avoid the crack of film and to increase the thickness of single layer, polyvinylpyrrolidone (PVP) with an average molecular weight of 40,000 was subsequently added to the precursor solution, and the molar ratio of PVP monomer to PLZST was 1:1. The concentration of the precursor solution was 0.5 M. After aged for 24 h, PLZST AFE film was deposited on $LaNiO_3$/Si (100) substrates through a multiple-step spin-coating technique. Each layer was spin coated at 3000 rpm for 40 s. In order to reduce the formation of cracks, every wet film was first dried at 300 ^oC for 10 min and subsequently pyrolyzed at 700 ^oC for 10 min. The spin-coating and heat-treatment were repeated six times to obtain the desired thickness. To prevent excessive lead loss and form pure perovskite phase, a capping layer of 0.4 M PbO precursor solution which was prepared from lead acetate trihydrate was deposited on the top of the PLZST film before it went through a final anneal at 700 ^oC for 30 min. The final thickness of all the PLZST AFE thick film was about 2 μm.

The microstructure of the PLZST AFE thick film was analyzed by X-ray diffraction (XRD Bruker D8 Advanced Diffractometer, German) and field-emission scanning electron microscopy (FE-SEM ZEISS Supra 55, German), respectively. For the electrical measurements, gold pads of 0.20 mm in diameter were coated on the film surface as top electrodes by using a DC sputtering method. The temperature-dependent dielectric properties of the film were measured by using a

computer-controlled Agilent E4980A LCR analyzer. The polarization-electric field hysteresis loops (*P-E*) at 1 kHz and the leakage current characteristic of the film were measured by a Ferroelectric tester (Radiant Technologies, Inc., Albuquerque, NM).

4. Conclusions

The ECE of PVP-modified sol-gel derived AFE PLZST thick film was investigated. Giant ECE values (ΔT = 53.8 ^{o}C and ΔS = 63.9 J·K^{-1}·kg^{-1}) at 5 ^{o}C rather than at T_c (195 ^{o}C) was received due to the AFE-FE phase switching. Accordingly, the maximum electrocaloric coefficient of 0.060 K·cm/kV and refrigeration efficiency of 18 were also obtained at 5 ^{o}C in the AFE thick film, which indicated that AFEs possessed acceptable cooling performance. At room temperature, the values of ΔT, ΔS, *COP* and ξ_{max} were 35.0 ^{o}C, 39.0 J·K^{-1}·kg^{-1}, 14 and 0.039 K·cm/kV at 900 kV/cm, respectively. Field-induced AFE-FE phase transition plays a key role in the dramatic ECE in the AFEs, in contrast to the AFE-PE phase transition. These results indicate that the AFEs have the potential for the applications in cooling devices near room temperature.

Acknowledgement

The authors would like to acknowledge the financial support the Program for New Century Excellent Talents in University (2012), the National Natural Science Foundation of China under grant No. 51462027, the Ministry of Sciences and Technology of China through 973-project under grant No.2014CB660811, and the Grassland Talent Plan of Inner Mongolia Autonomous Region, the Program for Young Talents of Science and Technology in Universities of Inner Mongolia Autonomous Region, and the Postgraduate Innovation Fund of Inner Mongolia Autonomous Region (No.20141012708).

Reference

[1] F. Jona, and G. Shirane, *Ferroelectric Crystals*, Dover Publications, Inc: New York, 1993.

[2] X. Moya, E. Stern-Taulats, S. Crossley, D. González-Alonso, S. Kar-Narayan, A. Planes, L. Mañosa, and N. D. Mathur, *Adv. Mater.*, 2013, **25**, 1360-1365.

[3] S. Lang, *Ferroelectrics.*, 1976, **11**, 519-523.

[4] X. S. Qian, H. J. Ye, Y. T. Zhang, H. M. Gu, X. Y. Li, C. A. Randall, and Q. M. Zhang, *Adv. Funct. Mater*., 2014, **24**, 1300-1305.

[5] Y. Bai, G. P. Zheng, and S. Q. Shi, *Appl. Phys. Lett.*, 2010, **96**, 192902.

[6] S. G. Lu, B. Rožič, Q. M. Zhang, Z. Kutnjak, X. Y. Li, E. Furman, L. J. Gorny, M. R. Lin, B. Malič, M. Kosec, R. Blinc, and R. Pirc, *Appl. Phys. Lett.*, 2010, **97**, 162904.

[7] A. S. Mischenko, Q. Zhang, J. F. Scott, R. W. Whatmore, and N. D. Mathur, *Science*, 2006, **311**, 1270-1271.

[8] S. G. Lu, Q. M. Zhang, *Adv. Mater.*, 2009, **21**, 1983-1987.

[9] P. Kobeko, and J. Kurtschatov, *Z. Phys.* 1930, **66**, 192-205.

[10] G. G. Wiseman, and J. Kuebler, *Phys. Rev.*, 1963, **131**, 2023-2027.

[11] T B. A. Tuttle, and D. A. Payne, *Ferroelectrics*, 1981, **37**, 603-606.

[12] D. Saranya, A. R. Chaudhuri, J. Parui, and S.B. Krupanidhi, *Bull. Mater. Sci.*, 2009, **32**, 259-262.

[13] B. L. Peng, H. Q. Fan, and Q. Zhang, *Adv. Funct. Mater.*, 2013, **23**, 2987-2992.

[14] X. H. Hao, J. W. Zhai, L. B. Kong, and Z. K. Xu, *Prog. Mater. Sci.*, 2014, **62**, 1-57.

[15] S. Corkovic, and Q. Zhang, *J. Appl. Phys.,* 2009, **105**, 061610.

[16] P. D. Thacher, *J. Appl. Phys.*, 1968, **39**, 1996-2002.

[17] B. M. Xu, Y. H. Ye, and L. E. Cross, *J. Appl. Phys.,* 2000, **87**, 2507-2515.

[18] Z. H. Du, T. S. Zhang, and J. Ma, *J. Mater. Res.*, 2007, **22**, 2195-2203.

[19] G. T. Park, J. J. Choi, C. S. Park, J. W. Lee, and H. E. Kim, *Appl. Phys. Lett.*, 2004, **85**, 2322-2324.

[20] Y. B. Shi, B. Liu, P. Q. Li, X. J. Chou, Z. M. Ma, C. Y. Xue, and J. Liu, *Ceram. Int.*, 2014, **40**, 10915-10918.

[21] X. H. Hao, Z. X. Yue, J. B. Xu, S. L. An, and C. W. Nan, *J. Appl. Phys.*, 2011, **110**, 064109.

[22] T. Mitsui, I. Tatsuzaki, and E. Nakamura, *An introduction to the physics of ferroelectrics*, Gordon and Breach, Landon, 1976.

[23] B. Neese, B. J. Chu, S. G. Lu, Y. Wang, E. Furman, and Q. M. Zhang, *Science*, 2008, **321**, 821-823.

[24] E. Defay, S. Crossley, S. K. Narayan, X. Moya, and N. D. Mathur, *Adv. Mater.*, 2013, **25**, 3337-3342.

[25] D. Saranya, J. Parui, and S. B. Krupanidhi, *Ferroelectrics*, 2013, **453**, 38-43.

[26] J. F. Wang, T. Q. Yang, K. Wei, and X. Yao, *Appl. Phys. Lett.*, 2013, **102**, 152907.

[27] X. J. Jiang, L. H. Luo, B. Y. Wang, W. P. Li, and H. B. Chen, *Ceram. Int.,* 2014, **40**, 2627-2634.

[28] M. A. Hamad, *Appl. Phys. Lett.*, 2013, **102**, 142908.

[29] G. Singh, I. Bhaumik, S. Ganesamoorthy, R. Bhatt, A.K. Karnal, V. S. Tiwari, and P. K. Gupta, *Appl. Phys. Lett.*, 2013, **102**, 082902.

[30] B. Li, W. J. Ren, X. W. Wang, H. Meng, X. G. Liu, Z. J. Wang, and Z. D. Zhang, *Appl. Phys. Lett.*, 2010, **96**, 102903.

[31] B. Ma, D. K. Kwon, M. Narayanan, and U. B. Balachandran, *J. Phys. D: Appl. Phys.*, 2008, **41**, 205003.

[32] L. Zhang, and X. H. Hao, *J. Alloys Comp.*, 2014, **586**, 674-678.

Figure Caption

Fig. 1 Schematic drawing of the ECE process of AFEs and FEs upon withdrawal of external electric field.

Fig. 2 XRD pattern of the PLZST AFE thick film. The inset is the surface (a) and cross-section (b) FE-SEM images of this thick film.

Fig. 3 Temperature dependence of dielectric constant of PLZST AFE thick film. The inset is the room temperature frequency-dependent dielectric constant and dielectric loss of the thick film.

Fig. 4 The *P-E* loops of the PLZST AFE thick film at different temperature. The inset is the electric field-dependent dielectric constant of thick film at 100 kHz.

Fig. 5 (a) Temperature ΔT as a function of temperature under various applied electric field E of the PLZST AFE thick film and (b) The adiabatic changes in entropy ΔS. The inset in Fig. 5 (a) is maximum polarization as a function of temperature under different electric field of the sample.

Fig. 6 The temperature dependence of the electrocaloric coefficient and refrigeration efficiency.

Fig. 7 The leakage current density and the resistivity as a function of time of the PLZST AFE thick film at different temperature. The inset is the corresponding temperature dependences of steady-state leakage current density.

Fig. 1 Ye Zhao, and Xihong Hao, *et.al.*

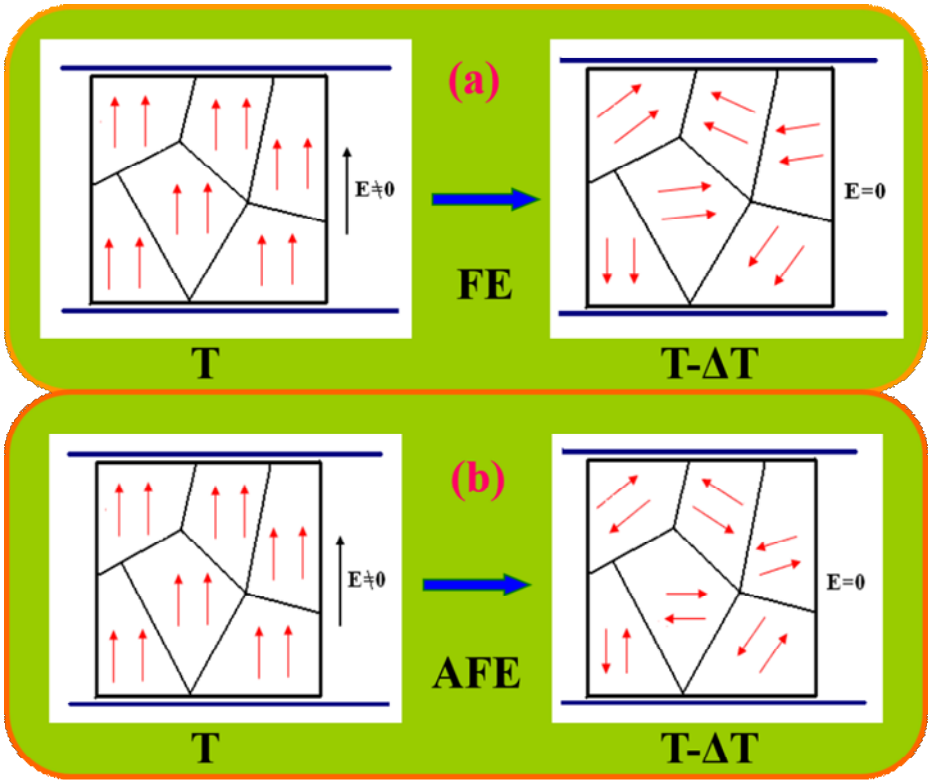

Fig. 2 Ye Zhao, and Xihong Hao, *et.al.*

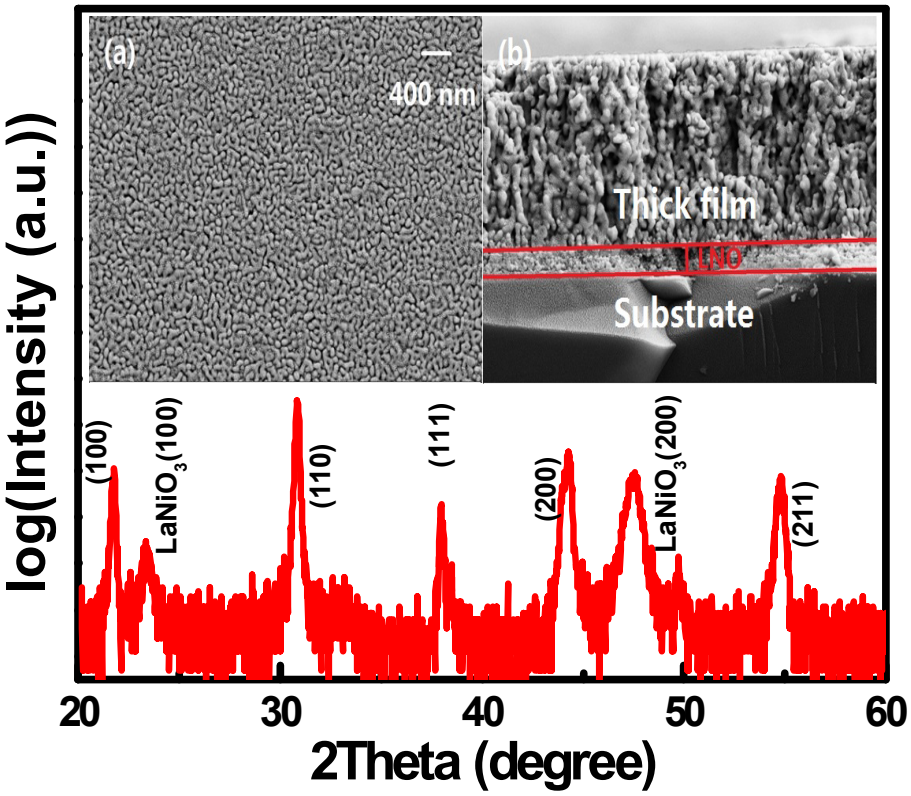

Fig. 3 Ye Zhao, and Xihong Hao, *et.al.*

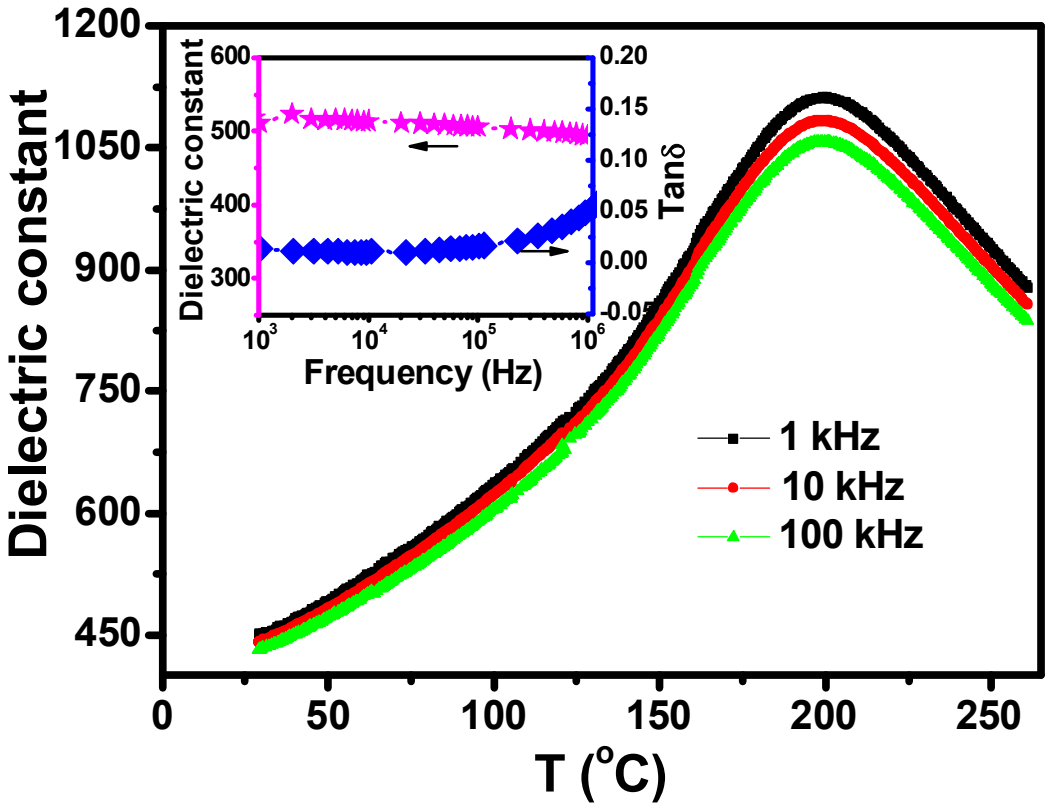

Fig. 4 Ye Zhao, and Xihong Hao, *et.al.*

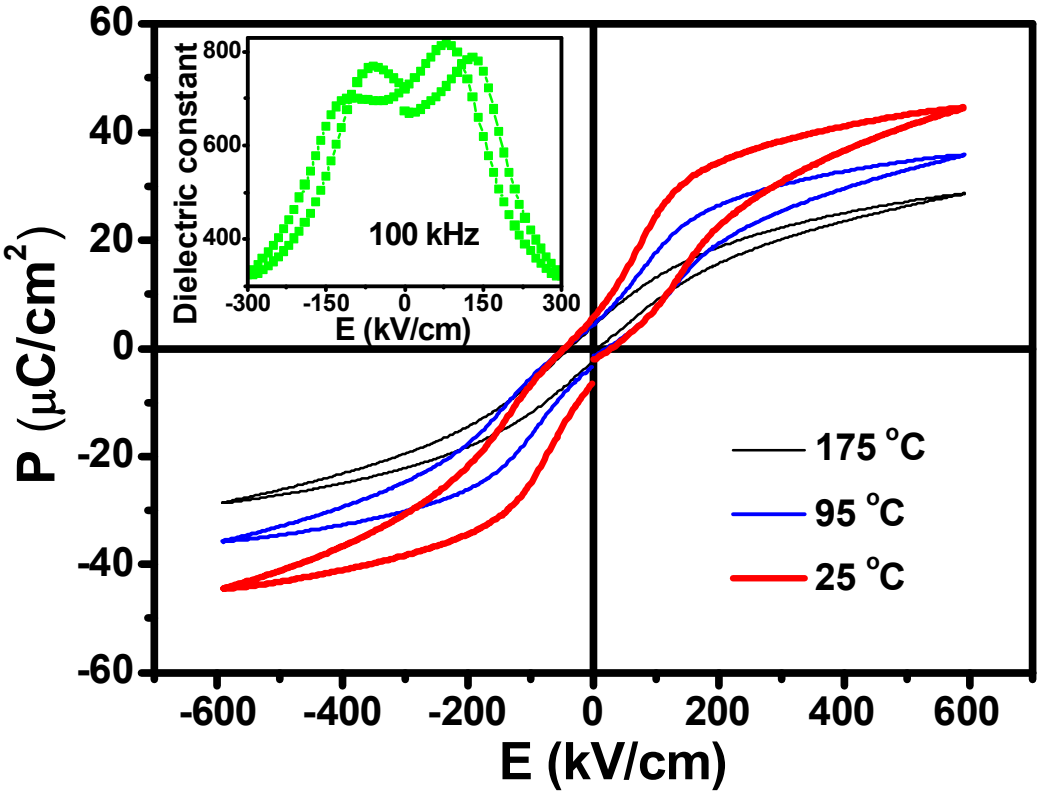

Fig. 5 Ye Zhao, and Xihong Hao, *et.al.*

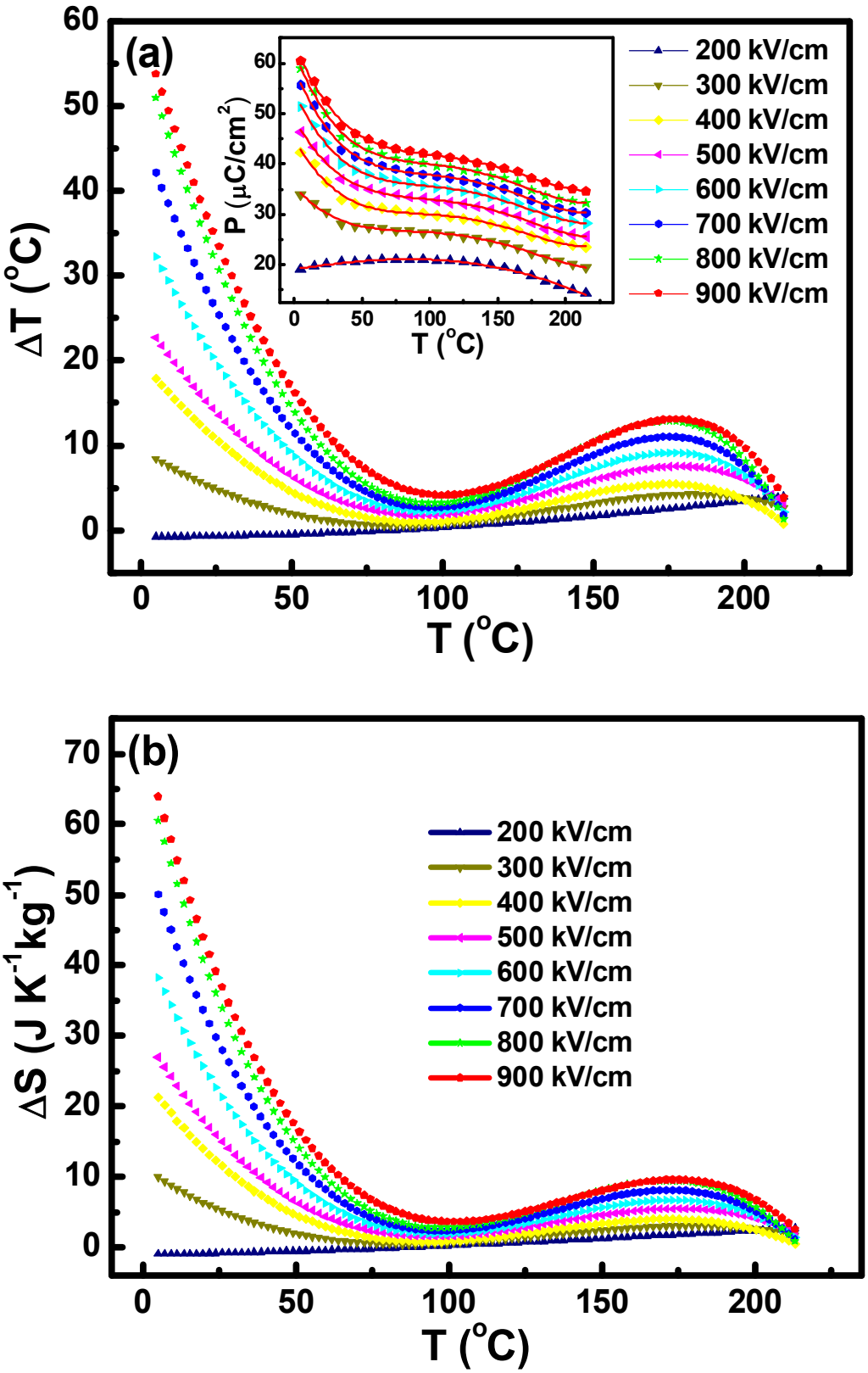

Fig. 6 Ye Zhao, and Xihong Hao, *et.al.*

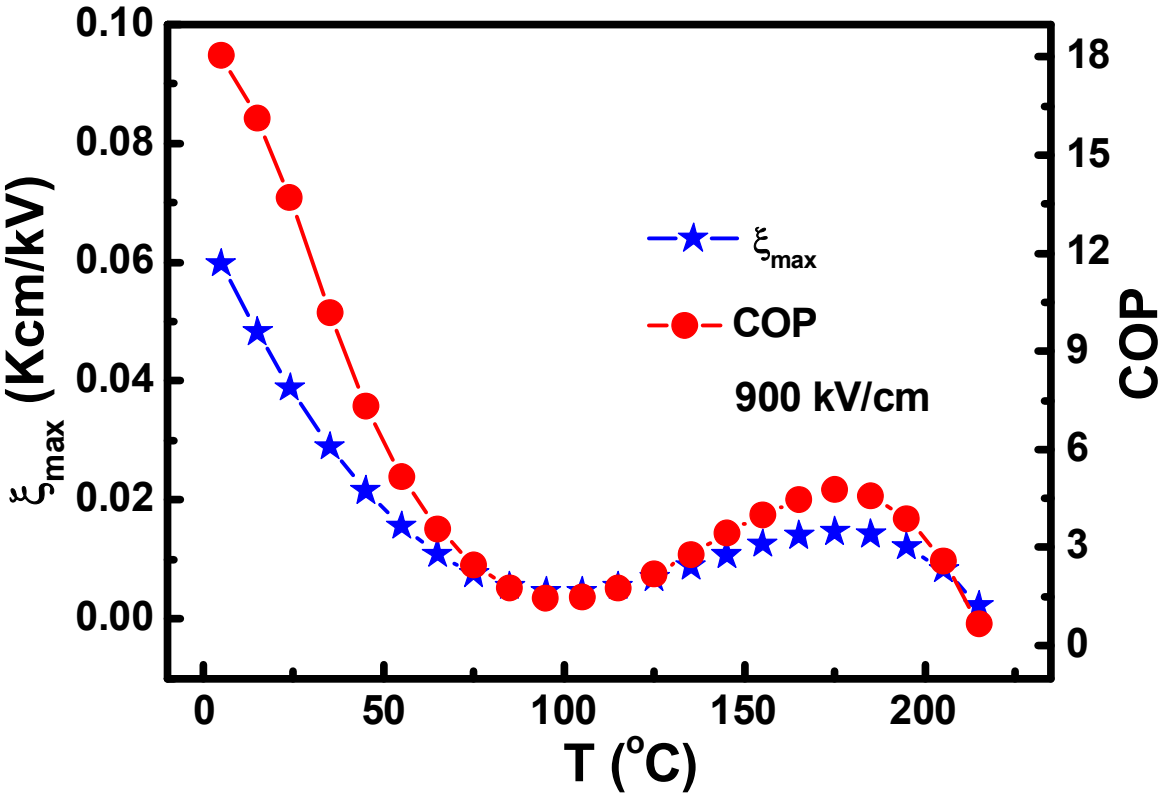

Fig. 7 Ye Zhao, and Xihong Hao, *et.al.*

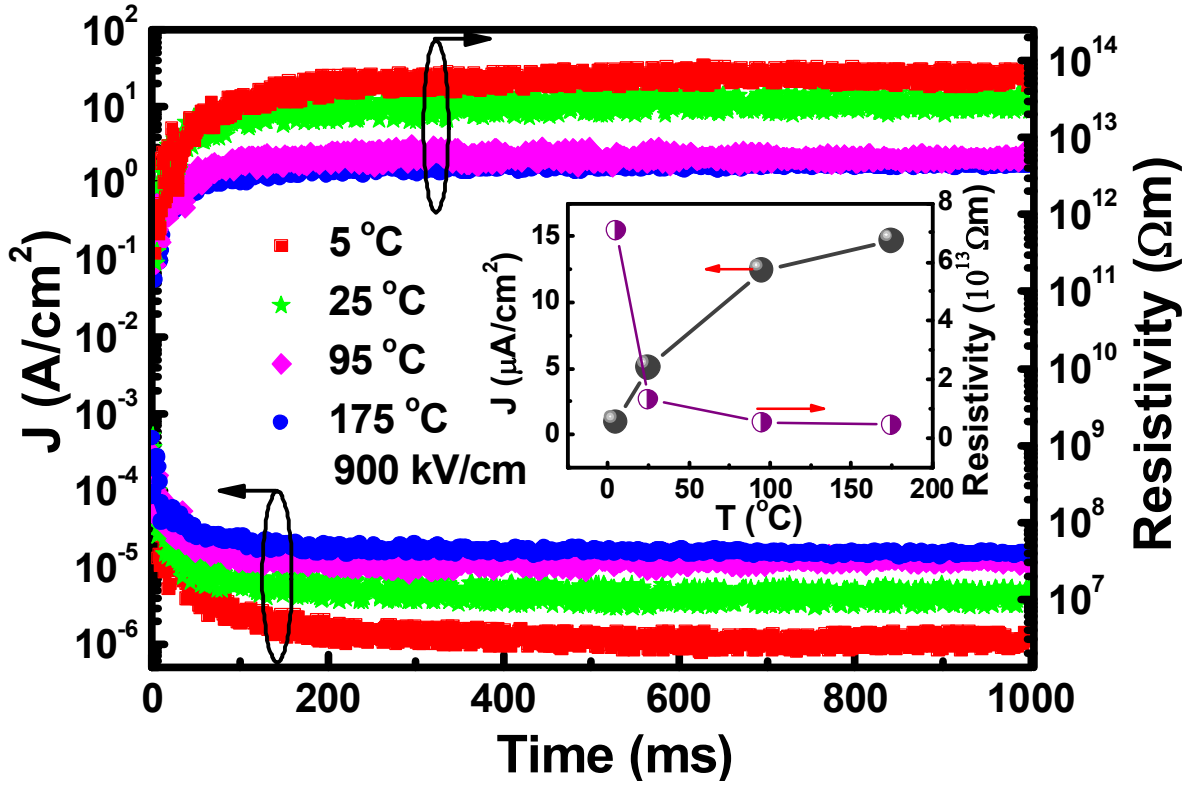

Table 1. (Electrocaloric characteristics of films, polymers, ceramics and single crystals.)

Material	Thickness (μm)	ΔT (°C)	COP	ξ_{max} (K·cm/kV)	RC ($J \cdot kg^{-1}$)	Phase transition	T (°C)	Ref.
PLZST film	2	53.8	18	0.060	3438	AFE-FE	5	This work
PLZST film	2	35.0	14	0.039	1365	AFE-FE	25	This work
$PbZr_{0.95}Ti_{0.05}O_3$ film	0.35	12	3	0.025	96	AFE-PE	226	[7]
P(VDF–TrFE) film	0.4-2	12.6	7.5	0.006	756	FE-PE	80	[23]
P(VDF-TrFE–CFE) film	0.4-2	12	–	0.004	660	FE-PE	55	[23]
$Pb_{0.80}Ba_{0.20}ZrO_3$ film	0.32	45.3	–	0.076	2125	AFE-FE	17	[13]
0.85PMN-0.15PT film	0.5	4	–	0.010	–	FE-PE	-20	[25]
$Pb_{0.99}Nb_{0.02}(Zr_{0.75}Sn_{0.20}Ti_{0.05})_{0.98}O_3$ ceramic	–	2.5	–	0.083	–	FE-PE	161	[11]
$Pb(Zr_{0.455}Sn_{0.455}Ti_{0.09})O_3$ ceramic	–	1.6	–	0.053	–	AFE-FE	55	[16]
$BaZr_{0.2}Ti_{0.8}O_3$ ceramic	–	4.5	–	0.31	–	–	39	[4]
PZT-5 ceramic	–	0.15	–	0.005	–	–	25	[26]
$0.94Bi_{0.5}Na_{0.5}TiO_3–0.06KNbO_3$ ceramic	–	1.73	–	0.025	–	depolarization	76	[27]
$Pb(Mg_{0.067}Nb_{0.133}Zr_{0.8})O_3$ ceramic	–	0.91	–	0.046	40.69	FE-PE	200	[28]
$0.45Ba_{0.2}Ti_{0.8}O_3$-$0.55Ba_{0.7}Ca_{0.3}TiO_3$ single crystal	–	0.46	–	0.038	–	FE-PE	131	[29]

¶